Enhancing Dielectric and Ferroelectric Properties in PFN–PT Ceramics via (Ca,Sr)ZrO_3 Modification for Advanced Electronic Applications

Marjaneh Jafari Fesharaki

Department of Physics, Payame Noor University, P. O. Box 19395-3697, Tehran, Iran

Email: M.Jafari.Fesharaki@pnu.ac.ir

Abstract

The structural, dielectric, and ferroelectric properties of (1−x)PFN–PT/x(Ca,Sr)ZrO_3 ceramics (x = 0–0.08) were systematically investigated. X-ray diffraction analysis confirmed the formation of a single-phase perovskite structure, while Rietveld refinement revealed a gradual reduction in the monoclinic lattice distortion with increasing CZ and SZ contents, indicating structural evolution toward a pseudocubic-like state near the morphotropic phase boundary (MPB). Quantitative FE-SEM analysis showed dense microstructures with progressive grain refinement at higher modifier concentrations. Temperature-dependent dielectric measurements exhibited the highest dielectric constant for the x = 0.04 compositions, whereas the modified Curie–Weiss analysis confirmed diffuse phase transition and relaxor behavior, with γ values of 1.94 and 1.68 for PFN–PT:0.04CZ and PFN–PT:0.04SZ, respectively. Room-temperature ferroelectric measurements yielded maximum remanent polarization (P_r) values of 24.32 and 34.26 μC cm^{-2} for the CZ- and SZ-modified ceramics at x = 0.04. The enhanced dielectric and ferroelectric properties are closely correlated with the reduced monoclinic distortion near the MPB, highlighting the crucial role of structural optimization in improving the functional performance of PFN–PT-based ceramics.

Key words: PFN-PT ceramics; $CaZrO_3$/$SrZrO_3$ modification; Morphotropic phase boundary (MPB); Dielectric and ferroelectric properties; Relaxor ferroelectrics.

1. Introduction

Ferroelectric ceramics constitute an important class of dielectric materials due to their unique polarization behavior and strong electromechanical coupling, enabling widespread applications in electronic devices such as actuators, capacitors, sensors, and non-volatile memory systems. Owing to their multifunctional properties and technological relevance, these materials have attracted sustained scientific interest and continue to play a significant role in modern electronic industries [1-3]. A fundamental challenge in employing ferroelectric ceramics as dielectric capacitors for power electronics and energy storage applications is maintaining stable performance under demanding operational conditions, particularly with respect to temperature stability and high dielectric permittivity [4, 5]. Among various material systems,

[DOI: 10.22068/ijmse.4601]

perovskite-based multiferroic oxides have attracted considerable attention due to their structural flexibility and the coexistence of multiple ferroic order parameters, which provide opportunities for tuning dielectric and ferroelectric responses across a wide temperature range [6, 7].

Lead iron niobate, $PbFe_{0.5}Nb_{0.5}O_3$ (PFN), is a lead-based complex multiferroic perovskite that has attracted considerable attention for multilayer capacitor applications due to its high dielectric constant, diffuse phase transition behavior, and relatively low sintering temperature [8, 9]. These characteristics are closely related to those observed in well-known lead-based relaxor ferroelectric systems such as $PbMg_{1/3}Nb_{2/3}O_3$–$PbTiO_3$ (PMN-PT) [10] and $PbZn_{1/3}Nb_{2/3}O_3$–$PbTiO_3$ (PZN-PT) [11], which are widely recognized for their outstanding dielectric and piezoelectric properties.

Structurally similar to PMN and PZN, PFN crystallizes in a rhombohedral structure at room temperature and undergoes a series of phase transitions upon cooling. Specifically, PFN transforms from a cubic paraelectric phase to a tetragonal ferroelectric phase at $T_C \approx 370$ K, followed by a transition to a rhombohedral (or monoclinic) ferroelectric phase at $T_1 \approx 350$ to 360 K, and finally to an antiferromagnetic phase below the N′eel temperature $T_N \approx 150$ K [12]. This sequence of phase transitions reflects a diffuse ferroelectric behavior that lies between normal ferroelectric and relaxor characteristics.

To improve the ferroelectric and piezoelectric properties of PFN, extensive efforts have been devoted to forming solid solutions with various perovskite compounds, including $Pb(Ni_{1/3}Nb_{2/3})O_3$ [13], $Pb(Zn_{1/3}Nb_{2/3})O_3$ [14], and notably $PbTiO_3$ (PT) have been explored [15]. Among these systems, the (1–x)PFN–xPT solid solution exhibits a morphotropic phase boundary (MPB), analogous to that observed in the classical $Pb(Zr_xTi_{1-x})O_3$ (PZT) system, which is known to promote enhanced functional properties.

The presence of a morphotropic phase boundary (MPB) is of considerable technological importance, as it is well known to maximize dielectric and piezoelectric responses in adjacent ferroelectric phases through enhanced polarization rotation and domain mobility [16, 17]. Consequently, chemical modification, particularly through the formation of perovskite solid solutions, has been widely employed as an effective approach to further optimize functional properties. In this context, the construction of ternary perovskite systems by incorporating an additional oxide end-member offers increased structural flexibility and provides new opportunities for fine-tuning phase stability and electrical performance.

Incorporation of an appropriate third component, such as $CaZrO_3$ (CZ) or $SrZrO_3$ (SZ), provides a purposeful route for further performance enhancement in ferroelectric ceramics. One notable consequence of such chemical modification is the induction of a ferroelectric-to-relaxor phase transition, which can be driven by a reduction in the Goldschmidt tolerance factor (t) through selective ionic substitution [18].

[DOI: 10.22068/ijmse.4601]

The tolerance factor, defined as $t = (R_A + R_O)/\sqrt{2}\,(R_B + R_O)$, where R_A, R_B and R_O represent the ionic radii of the A-site cation, B-site cation, and oxygen anion, respectively, is a critical parameter governing the structural stability and lattice distortion of ABO_3-type perovskites [19]. Substitution of smaller ions at the A-site and/or larger ions at the B site effectively reduces the tolerance factor, thereby promoting structural instability and enhanced dielectric relaxation behavior.

Substitution of smaller ions at the A-site and/or larger ions at the B site effectively reduces the tolerance factor, thereby promoting structural instability and enhanced dielectric relaxation behavior. Such local structural modifications also influence the lattice distortion and the free-energy landscape of competing ferroelectric phases. Consequently, compositions approaching the morphotropic phase boundary (MPB) facilitate polarization rotation and domain switching, which are widely recognized as the primary microscopic mechanisms responsible for enhanced dielectric and ferroelectric properties [16,17].

In this regard, CZ and SZ are widely employed perovskite modifiers owing to their proven effectiveness in stabilizing crystal structures, tuning phase boundaries, and improving the dielectric and ferroelectric properties of lead-based perovskite ceramics [20- 26].

Mathematically, introducing CZ and SZ-with smaller A-site cations (R_{Ca} = 0.99 ˚A, R_{Sr} = 1.12 ˚A <R_{Pb} = 1.19 ˚A) and larger B-site ions (R_{Zr} = 0.72 ˚A > R_{Fe} = 0.645 ˚A, R_{Nb} = 0.64 ˚A, R_{Ti} = 0.605 ˚A)—is expected to reduce the tolerance factor, distort the perovskite lattice, and induce relaxor-like dielectric behavior in the PFN–PT host. While several studies have explored the ferroelectric properties of PFN–PT [27- 32], no reports exist on CZ or SZ-modified (1-x)PFN-xPT multiferroics.

In this study, (1–x)PFN–PT/xCZ(SZ) ceramics (x = 0–0.08) were synthesized via a solid-state reaction method. The structural, dielectric, and ferroelectric properties were systematically investigated to elucidate the effects of CZ and SZ modification on phase structure, dielectric response, and remanent polarization, with a focus on enhancing functional performance.

2. Experimental Procedure

Pure $CaZrO_3$ (CZ) and $SrZrO_3$ (SZ) powders were synthesized via a sol–gel auto-combustion method, as described in Ref. [33], to obtain nanocrystalline particles suitable for modification of PFN–PT ceramics. The polycrystalline $0.94[Pb(Fe_{0.5}Nb_{0.5})O_3]$–$0.06PbTiO_3$ (PFN–PT) powders were prepared by a conventional solid-state reaction method. High-purity PbO (with 4 wt.% excess to compensate for lead volatilization during high-temperature sintering), Fe_2O_3, Nb_2O_5, TiO_2, and 1 wt.% Li_2CO_3 (added to reduce electronic conduction) were used as starting materials. Stoichiometric amounts of the raw powders were mixed and manually ground for 1.5 h using an agate mortar to ensure homogeneity. The PFN–PT powders

[DOI: 10.22068/ijmse.4601]

were calcined in a two-step process: first at 900 °C for 4 h and then at 1000 °C for 7 h to promote complete phase formation. Composite powders of (1−x)PFN–PT:xCZ(SZ) (x = 0.02, 0.04, 0.06, and 0.08) were prepared by thoroughly mixing the CZ(SZ) and PFN–PT powders in ethanol using ball milling for 24 h. The mixtures were dried, pressed into pellets (8 mm in diameter and approximately 1 mm in thickness) under a hydraulic press, and finally sintered at 970 °C for 3 h in ambient atmosphere to obtain dense ceramics.

The crystal structures of the sintered samples were characterized by X-ray diffraction (XRD) using Cu-Kα radiation (Empyrean diffractometer). Structural parameters, including lattice constants, unit-cell volume, X-ray density, and lattice distortion, were determined by Rietveld refinement using the MAUD software. The microstructures and grain size distributions were examined by field-emission scanning electron microscopy (FE-SEM). Temperature-dependent dielectric measurements (25–300 °C) of the real part of the permittivity (ε′) and dielectric loss (tanδ) were primarily carried out at 650 kHz using an LCR meter (IM3570, Hioki). To evaluate the frequency dependence of the optimized compositions (x = 0.04), additional dielectric measurements were performed at 10 kHz, 100 kHz, 650 kHz, and 1 MHz. Ferroelectric hysteresis loops were recorded at room temperature using a home-built polarization–electric field (P–E) measurement system based on the Sawyer–Tower circuit.

3. Results and Discussion

Figures 1(a) and 2(a) show the XRD patterns of (1−x)PFN–PT/xCZ and (1−x)PFN–PT/xSZ ceramics (x = 0.00–0.08), respectively. All diffraction patterns indicate the formation of a single-phase perovskite structure, with no detectable secondary phases, and are in good agreement with the standard JCPDS card No. 89-3128. This indicates that the incorporation of CZ or SZ does not disrupt the perovskite framework within the investigated composition range. A closer inspection of the (110) reflection around $2\theta \approx 32°$ (Figs. 1b and 2b) reveals a noticeable structural evolution with increasing modifier content. For the pristine PFN–PT sample (x = 0), the splitting of the (110) reflection is clearly observed, which is characteristic of a monoclinic crystal structure and indicates proximity to a monoclinic–pseudocubic morphotropic phase boundary (MPB), consistent with previous reports [34,35].

[DOI: 10.22068/ijmse.4601]

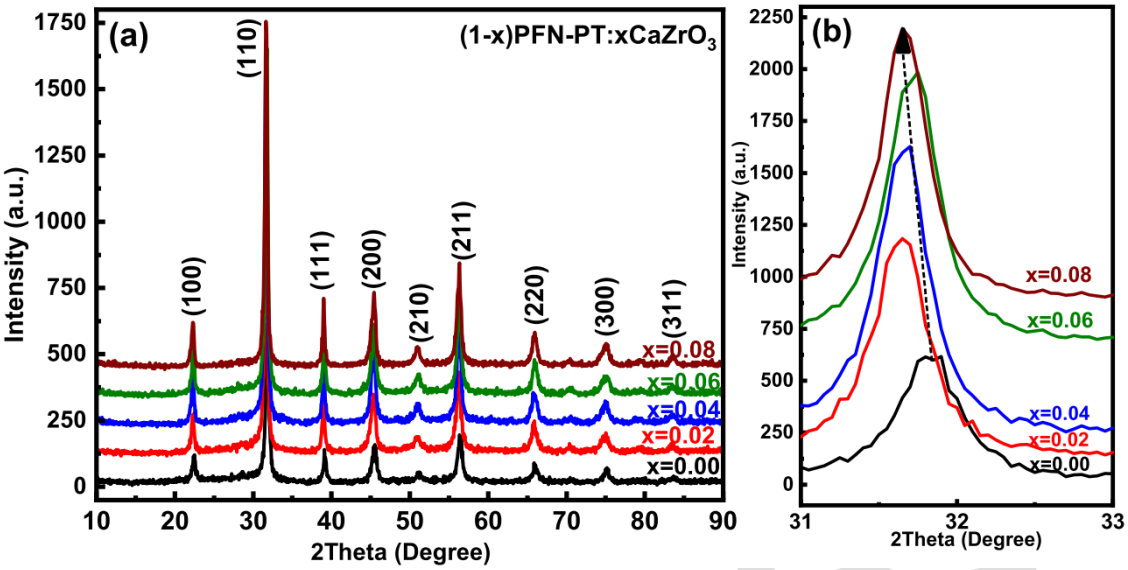

Fig. 1. XRD patterns of (1−x)PFN–PT/xCZ ceramics over the 2θ range of (a) 10–90° and (b) 31–33°.

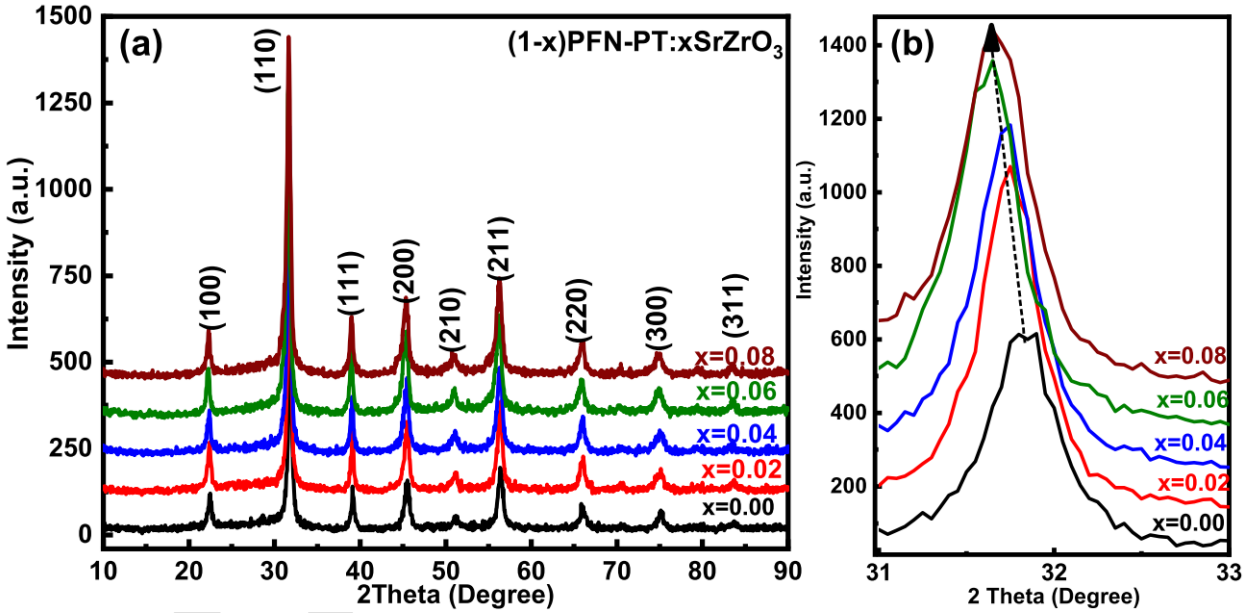

Fig. 2. XRD patterns of (1−x)PFN–PT/xSZ ceramics over the 2θ range of (a) 10–90° and (b) 31–33°.

Upon incorporation of CZ or SZ modifiers, the split diffraction peaks progressively merge into a single peak at x = 0.02, indicating a progressive reduction of the monoclinic distortion and the evolution toward a pseudocubic-like average structure, while confirming the formation of ternary PFN–PT–CZ(SZ) solid solutions. In addition, a systematic shift of the diffraction peaks toward lower 2θ angles is observed with increasing CZ/SZ content, suggesting the successful incorporation of the modifiers into the PFN–PT lattice, accompanied by a gradual expansion of the unit cell. Similar peak-shift behavior has been reported for

[DOI: 10.22068/ijmse.4601]

compositionally modified ferroelectric perovskites and is commonly associated with changes in lattice parameters [23,24,34,35].

To quantitatively evaluate the structural evolution, Rietveld refinement of the XRD data was performed using the MAUD program [36]. Figures 3 and 4 show representative refined diffraction patterns for the (1−x)PFN–PT and (1−x)PFN–PT compositions at x = 0.02. The quality of the refinements was evaluated using the goodness-of-fit parameter (GOF = Rwp/Rexp) together with the refinement reliability factors Rp, Rwp, and Rexp, which indicate satisfactory agreement between the observed and calculated diffraction profiles.

The refined structural parameters summarized in Tables I and II provide a quantitative description of the structural evolution induced by CZ and SZ incorporation. The lattice parameters (a, b, c), monoclinic angle (β), unit-cell volume (V), and X-ray density (ρ_x) exhibit systematic but relatively small variations with increasing modifier concentration, indicating that the perovskite framework remains structurally stable throughout the investigated composition range. Nevertheless, the difference between the a and b lattice parameters ($\Delta = |a - b|$), together with the monoclinic angle β, reveals a gradual reduction in the monoclinic lattice distortion. In particular, the minimum Δ values obtained around x = 0.04 indicate that the crystal structure progressively approaches a pseudocubic-like average structure while still being satisfactorily refined using the monoclinic Cm structural model. This structural evolution is fully consistent with the gradual merging of the split (110) reflection observed near $2\theta \approx 32°$, confirming that the incorporation of CZ or SZ progressively reduces the monoclinic distortion without altering the perovskite phase. The reduced monoclinic distortion reflects a decrease in lattice anisotropy, which is expected to facilitate polarization rotation in the vicinity of the morphotropic phase boundary (MPB) and provides the structural basis for the enhanced dielectric and ferroelectric properties discussed in the following sections [16,17].

[DOI: 10.22068/ijmse.4601]

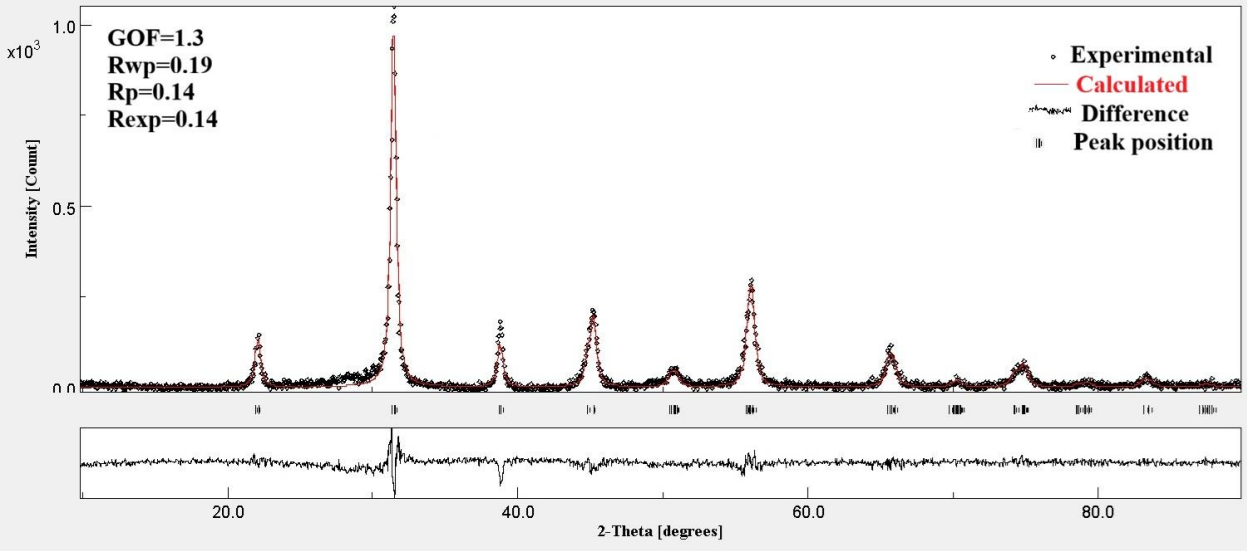

Fig. 3. Rietveld refinement plot of the XRD pattern of (1−x)PFN–PT/xCZ ceramics for x = 0.02.

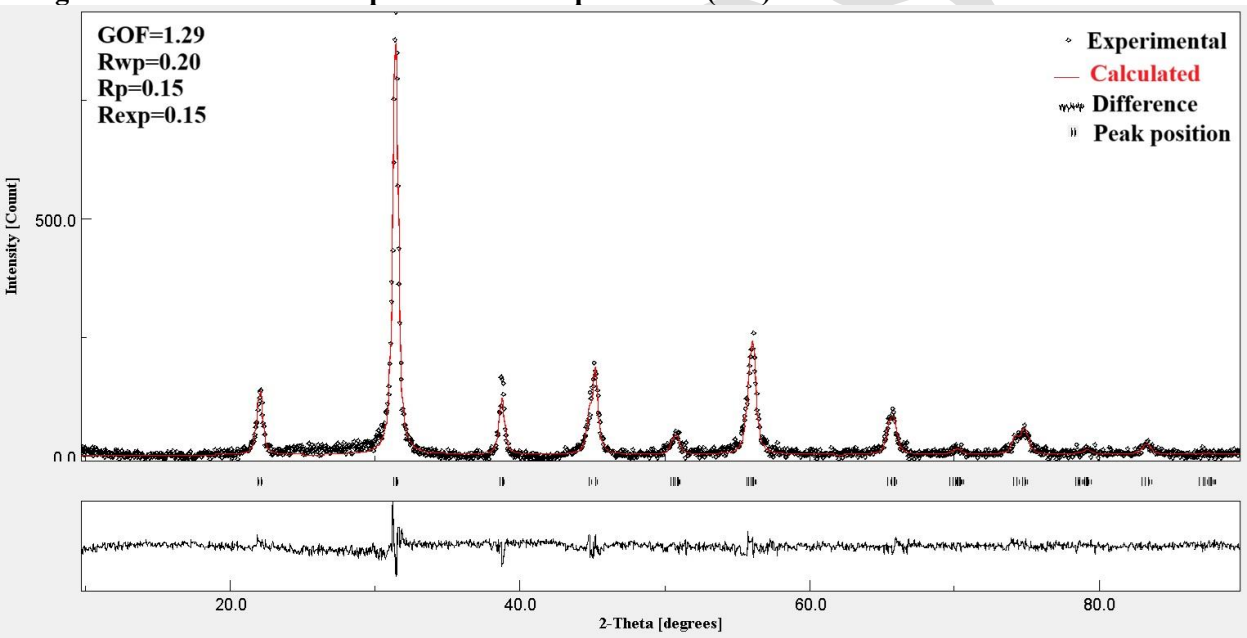

Fig. 4. Rietveld refinement plot of the XRD pattern of (1−x)PFN–PT/xSZ ceramics for x = 0.02

[DOI: 10.22068/ijmse.4601]

Table 1. Structural parameters of (1−x)PFN–PT/xCZ ceramics (x = 0, 0.02, 0.04, 0.06, and 0.08).

Parameter	x=0.0	x=0.02	x=0.04	x=0.06	x=0.08
a (Å)	5.6679	5.6608	5.6643	5.6648	5.6652
b (Å)	5.6751	5.6741	5.6647	5.6650	5.6616
c (Å)	4.0397	4.0426	4.0366	4.0401	4.0380
β (°)	89.80	90.13	89.79	90.11	89.79
$\Delta=\lvert a-b \rvert$ (Å)	0.0072	0.0133	0.0004	0.0002	0.0036
$V=a^2c$ ($Å^3$)	129.84	129.71	129.37	129.56	129.84
ρ_x(g/cm^3)	8.39	8.35	8.31	8.27	8.23
Space group	C1m1	C1m1	C1m1	C1m1	C1m1
Structure	Monoclinic	Pseudo-cubic	Pseudo-cubic	Pseudo-cubic	Pseudo-cubic

Table 1. Structural parameters of (1−x)PFN–PT/xSZ ceramics (x = 0, 0.02, 0.04, 0.06, and 0.08).

Parameter	**x=0.0**	**x=0.02**	**x=0.04**	**x=0.06**	**x=0.08**
a (Å)	5.6679	5.6715	5.6706	5.6783	5.6747
b (Å)	5.6751	5.6670	5.6687	5.6631	5.6685
c (Å)	4.0397	4.0430	4.0410	4.0430	4.0440
β (°)	89.80	89.74	89.77	89.59	89.65
$\Delta=\lvert a-b \rvert$ (Å)	0.0072	0.0045	0.0019	0.0152	0.0062
$V=a^2c$ ($Å^3$)	129.84	129.97	129.92	130.07	130.05
ρ_x(g/cm^3)	8.39	8.38	8.37	8.35	8.34
Space group	C1m1	C1m1	C1m1	C1m1	C1m1
Structure	Monoclinic	Pseudo-cubic	Pseudo-cubic	Pseudo-cubic	Pseudo-cubic

[DOI: 10.22068/ijmse.4601]

A comparison of the refined structural parameters further indicates that both CZ and SZ modifications drive the PFN–PT lattice toward a pseudocubic-like structural state; however, slight differences are observed in their structural evolution. The CZ-modified ceramics exhibit a more gradual and consistent reduction in the monoclinic distortion over the investigated composition range. In contrast, although the SZ-modified ceramics also show a pronounced decrease in the monoclinic distortion at low substitution levels, a slight recovery of the monoclinic distortion is observed at higher SZ concentrations, which is consistent with the reappearance of peak broadening and the shoulder-like feature of the (110) reflection. Nevertheless, both modifier systems retain the single-phase perovskite structure throughout the investigated composition range, demonstrating that CZ and SZ are successfully incorporated into the PFN–PT lattice without inducing secondary phase formation. These results suggest that $CaZrO_3$ promotes a more stable structural evolution toward the pseudocubic-like state, whereas $SrZrO_3$ retains a slightly higher degree of local lattice distortion at higher substitution levels.

The calculated X-ray density exhibits a slight decreasing trend with increasing CZ/SZ content, which is primarily attributed to the lower average molecular weight of the modified compositions, while the unit-cell volume remains nearly unchanged. This observation further confirms that the structural evolution is governed mainly by local lattice distortion rather than by significant lattice expansion.

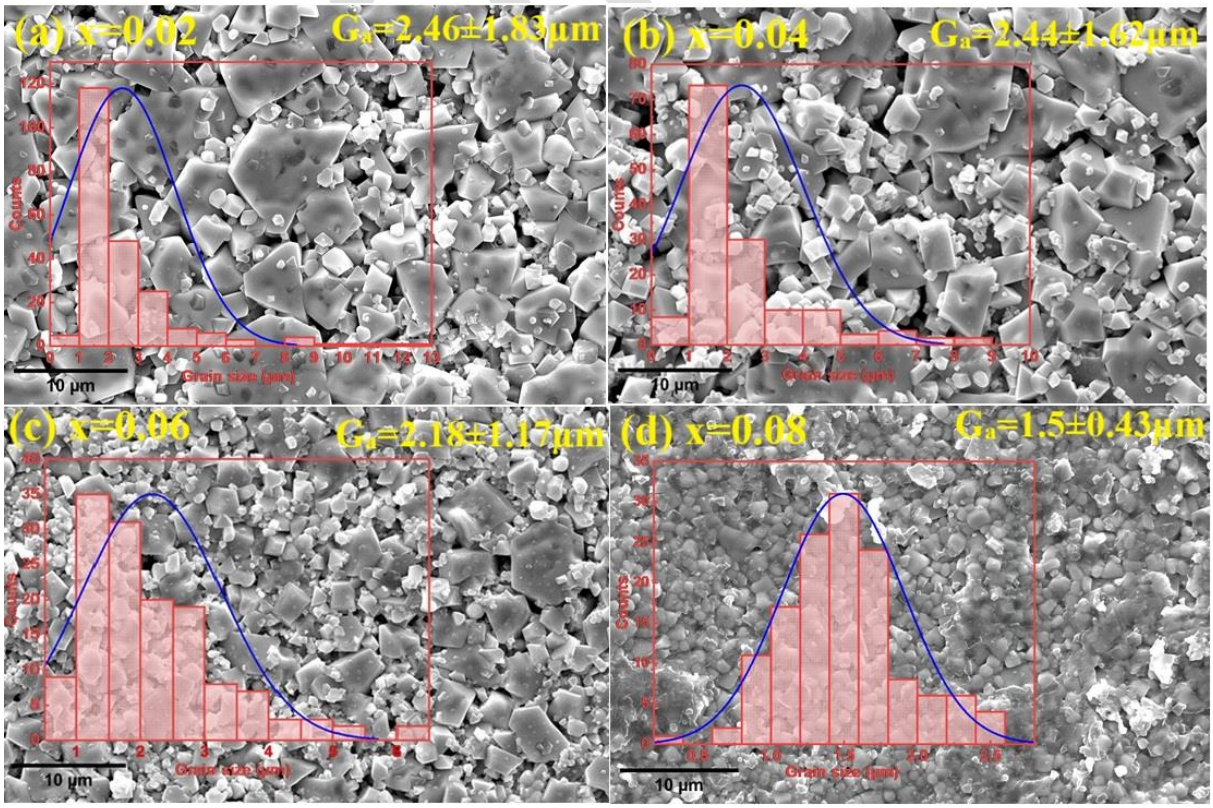

Fig. 5. FE-SEM micrographs of the (1-x)PFN–PT:xCZ ceramics.

[DOI: 10.22068/ijmse.4601]

Figure 5 shows the FE-SEM micrographs of the CZ-modified PFN-PT ceramics at different CZ contents. Quantitative grain-size analysis reveals that the average grain size remains nearly unchanged at low CZ contents (x = 0.02–0.04) but gradually decreases with further increasing CZ concentration, reaching its minimum value at x = 0.08. Moreover, the grain-size distribution becomes progressively narrower with increasing CZ content, indicating the development of a more homogeneous microstructure. This behavior suggests that CZ effectively suppresses grain growth during sintering, resulting in a finer and more uniform microstructure at higher CZ concentrations.

Figures 6(a) and 7(a) present the temperature dependence of the real part of the dielectric constant (ε′) for (1−x)PFN–PT/xCZ and (1−x)PFN–PT/xSZ ceramics, respectively, measured at 650 kHz. For both systems, ε′ increases with increasing CZ(SZ) content up to x = 0.04, beyond which a gradual decrease is observed. The maximum dielectric constant is obtained for compositions close to x = 0.04. This compositional dependence is in good agreement with the Rietveld refinement results, which revealed the minimum monoclinic distortion near x = 0.04. The reduced lattice anisotropy in the vicinity of the morphotropic phase boundary (MPB) facilitates polarization rotation, thereby enhancing the dielectric polarization and resulting in the highest dielectric constant.

As the temperature increases, ε′ gradually rises, reaches a broad maximum, and then decreases, indicating a diffuse ferroelectric–paraelectric phase transition rather than a sharp normal ferroelectric transition. The temperature corresponding to the maximum dielectric constant (T_m) was determined from the ε′–T curves. For the CZ-modified PFN–PT ceramics, T_m values of 133, 131, 106, 46, and 73 °C were obtained with increasing CZ content, whereas the corresponding values for the SZ-modified ceramics were 133, 109, 92, 71, and 38 °C. These transition temperatures are comparable to those previously reported for PFN–PT-based ceramics [12,37].

At higher modifier concentrations, the dielectric constant decreases for both systems, as shown in Figures 6(b) and 7(b). This reduction can be attributed to the deviation from the optimum MPB composition and the gradual increase in structural disorder, which weakens the cooperative polarization response. Table 3 compares the dielectric constants obtained in the present work with those reported for related PFN–PT-based ceramics, demonstrating the effectiveness of CZ and SZ modification in improving the dielectric performance

[DOI: 10.22068/ijmse.4601]

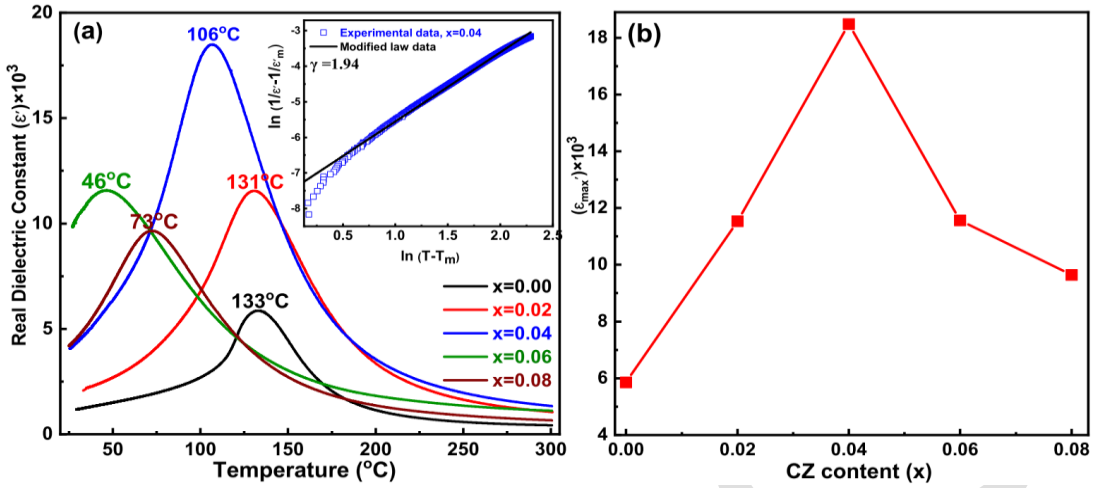

Fig. 6. (a) Temperature-dependent dielectric permittivity (ε′) of (1−x)PFN–PT/xCZ ceramics, and (b) variation of ε′ with CZ concentration.

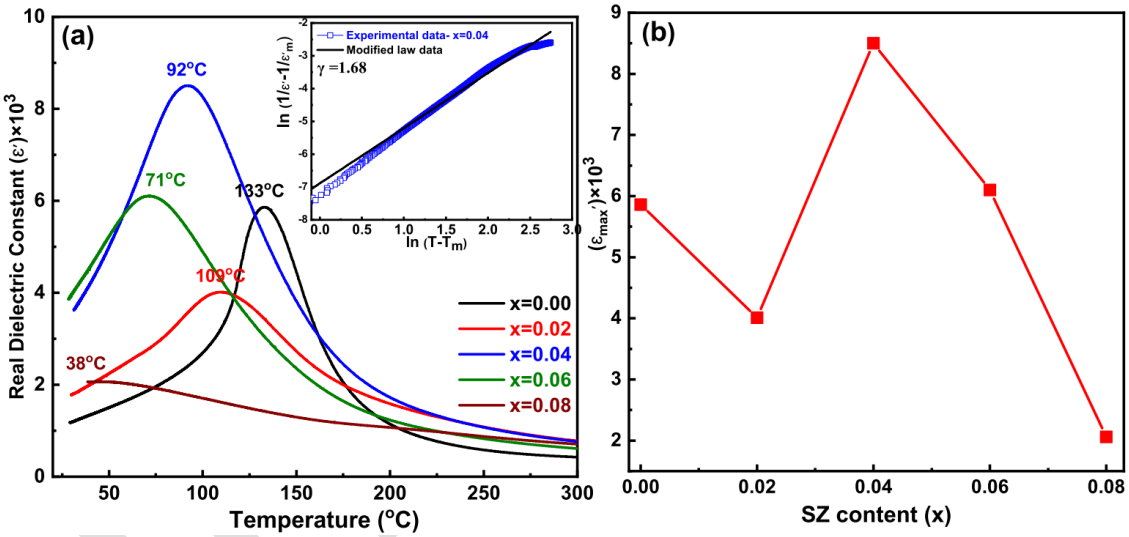

Fig. 7. (a) Temperature-dependent dielectric permittivity (ε′) of (1−x)PFN–PT/xSZ ceramics, and (b) variation of ε′ with SZ concentration.

Figure 8 presents the temperature dependence of the real part of the dielectric constant (ε′) measured at 10, 100, 650 kHz, and 1 MHz for the optimum CZ- and SZ-modified compositions (x = 0.04). For both ceramics, the dielectric constant gradually decreases with increasing frequency because the contributions from space-charge, interfacial, and domain-wall polarization become progressively less effective at higher frequencies. In contrast, the temperature corresponding to the dielectric maximum (T_m) remains nearly unchanged over the investigated frequency range, indicating that the dielectric dispersion mainly affects the magnitude of ε′ rather than the phase-transition temperature. Furthermore, the CZ-modified ceramic

[DOI: 10.22068/ijmse.4601]

exhibits consistently higher dielectric permittivity than the SZ-modified ceramic at all measured frequencies, although both systems display a similar frequency dependence.

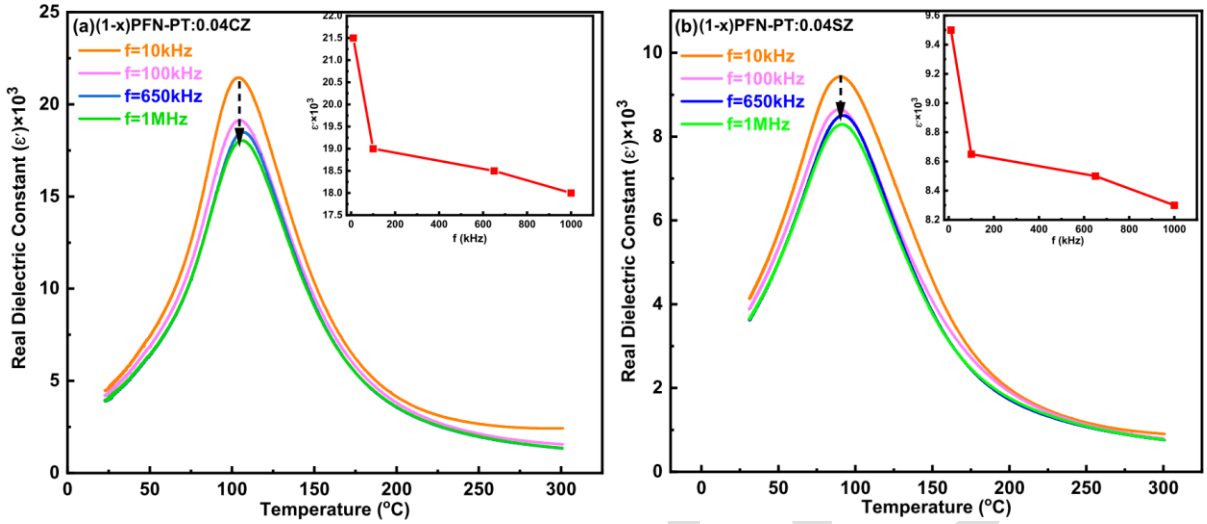

Fig. 8. Temperature dependence of the real part of dielectric permittivity (ε′) at different frequencies (10 kHz, 100 kHz, 650 kHz, and 1 MHz) for (a) PFN–PT:0.04CZ and (b) PFN–PT:0.04SZ ceramics.

The diffuseness of the ferroelectric phase transition was analyzed using the empirical modified Curie-Weiss law:

$$\frac{1}{\varepsilon'} - \frac{1}{\varepsilon'_m} = \frac{(T - T_m)^{\gamma}}{C_1}$$

where ε'_m, T_m, γ and C1 represent the maximum dielectric constant, transition temperature, diffusion coefficient, and Curie constant, respectively.

Table 3. Comparison of dielectric constant in relaxor ferroelectric ceramics.

Ceramics	Phase	έ	Ref
$0.1NdFeO_3$–$0.56Pb(Fe_{0.5}Nb_{0.5})O_3$–$0.34PbTiO_3$	MPB	1885	[7]
$0.02CaZrO_3$–$0.36BiScO_3$–$0.62PbTiO_3$	Tertagonal	1726	[23]
$0.11CaZrO_3$–$0.34Bi(Mg_{0.5}Ti_{0.5})O_3$–$0.55PbTiO_3$	Tetragonal	9000	[18]
$0.04CaZrO_3$–$0.9024Pb(Fe_{0.5}Nb_{0.5})O_3$–0.05766PbTiO3	Pseudo-cubic	18480	This Work
$0.04SrZrO_3$–$0.9024Pb(Fe_{0.5}Nb_{0.5})O_3$–0.05766PbTiO3	Pseudo-cubic	8480	This Work
$0.07SrZrO_3$–$0.90582(K_{0.5}Na_{0.5})NbO_3$–$0.02418Bi_{0.5}K_{0.5}TiO_3$	Tetragonal	6550	[25]
$0.02SrZrO_3$–$0.7105BiFeO_3$–$0.02695BaTiO_3$	MPB	5000	[24]

[DOI: 10.22068/ijmse.4601]

For normal ferroelectrics, $\gamma = 1$ while values between 1 and 2 indicate relaxor behavior, with $\gamma = 2$ corresponding to a completely diffuse phase transition [38-40]. The value of γ was determined from the slope of the linear fitting of- $\ln(1/\varepsilon' - 1/\varepsilon'_m)$ versus-$\ln(T - T_m)$, as shown in the insets of Figures 6(a) and 7(a) for measurements performed at 650 kHz. A good linear relationship is obtained for both compositions, yielding γ values of 1.94 and 1.68 for PFN-PT:0.04CZ and PFN-PT:0.04SZ, respectively. These values confirm the relaxor ferroelectric nature of both systems, with the CZ-modified ceramic exhibiting a stronger degree of diffuseness.

The observed relaxor behavior is attributed to the formation of polar nano-regions (PNRs) arising from the local structural disorder introduced by CZ(SZ) modification [39]. The substitution-induced lattice distortion and compositional fluctuations disrupt the long-range ferroelectric ordering and promote the formation of nanoscale polar regions, resulting in a broadened dielectric maximum and a diffuse phase transition. The larger (γ) value obtained for PFN–PT:0.04CZ is consistent with its stronger relaxor character compared with the corresponding SZ-modified composition.

Figures 9(a) and 9(b) show the temperature dependence of the dielectric loss ($\tan\delta$) for the CZ- and SZ-modified PFN–PT ceramics, respectively. The dielectric loss values are comparable to, or slightly lower than, those reported for related PFN–PT-based systems. Although no abrupt compositional dependence is observed, a slight overall decrease in dielectric loss with increasing CZ(SZ) content indicates that the modifiers improve the dielectric response without introducing excessive dielectric dissipation. As shown in the insets of Figures 9(a) and 9(b), the dielectric loss increases slightly with CZ(SZ) concentration at lower temperatures, which is attributed to defect-assisted charge transport associated with dopant incorporation [41–44]. At higher modifier concentrations, the dielectric behavior reflects the balance between defect-related conduction and the structural stabilization induced by CZ(SZ) incorporation.

[DOI: 10.22068/ijmse.4601]

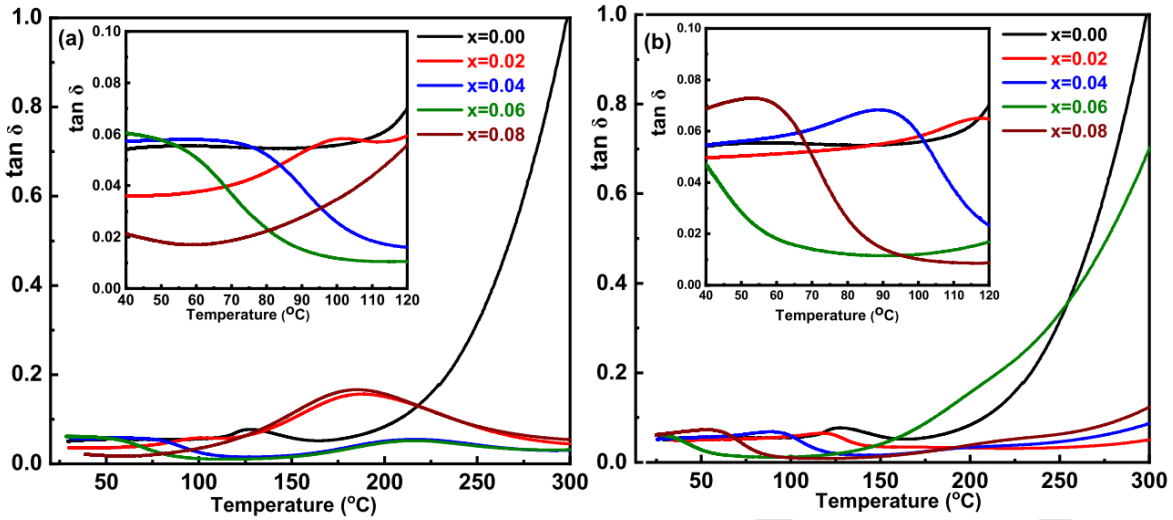

Fig. 9. Temperature dependence of dielectric loss tangent (tanδ) for (a) (1-x)PFN-PT:xCZ, and (b) (1-x)PFN-PT:xSZ ceramics.

Figures 10(a) and 11(a) show the room-temperature polarization–electric field (P–E) hysteresis loops of CZ- and SZ-modified PFN–PT ceramics, respectively. All compositions exhibit well-saturated hysteresis loops, confirming their ferroelectric behavior. The ferroelectric properties of PFN–PT-based solid solutions are strongly influenced by various factors, such as chemical composition, grain size, processing conditions, and sample geometry [24,44].

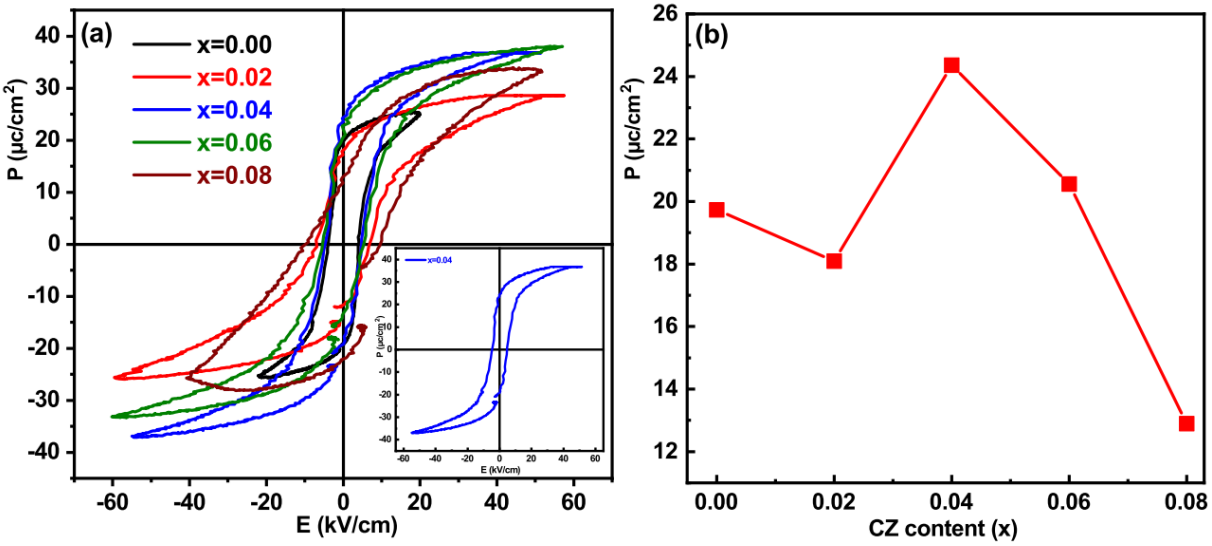

Fig. 10. (a) Room-temperature P–E hysteresis loops for PFN–PT:xCZ ceramics, and (b) composition dependence of remanent polarization (P_r) with CZ content.

[DOI: 10.22068/ijmse.4601]

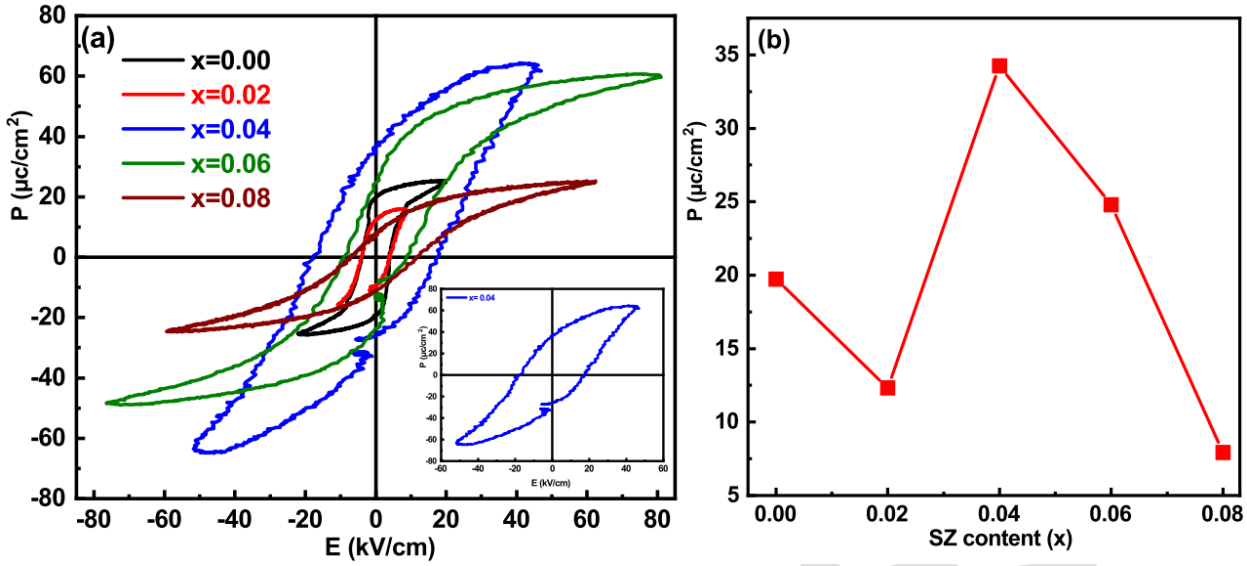

Fig. 11. (a) Room-temperature P–E hysteresis loops for PFN–PT:xSZ ceramics, and (b) composition dependence of remanent polarization (P_r) with SZ content.

As shown in Figures 10(b) and 11(b), the remanent polarization (Pr) initially increases with increasing CZ (SZ) content and reaches maximum values of 24.32 μC/cm² for PFN–PT:0.04CZ and 34.26 μC/cm² for PFN–PT:0.04SZ. These compositions correspond to the morphotropic phase boundary (MPB) region, as also supported by the enhanced dielectric constant observed in Figures 6(b) and 7(b). The coexistence of different structural phases near the MPB facilitates domain reorientation and polarization switching, resulting in an enhanced ferroelectric response. With further increase in CZ (SZ) concentration, a gradual decrease in Pr is observed. This reduction can be attributed to the deviation from the MPB region and the increased contribution of a pseudocubic phase, which may restrict long-range ferroelectric ordering and decrease the amount of switchable polarization. At higher dopant levels (x = 0.08), electrical breakdown occurs when the applied electric field exceeds approximately 4.7 kV/mm for PFN–PT:0.08CZ and 6.2 kV/mm for PFN–PT:0.08SZ, as shown in Figures 10(a) and 11(a). This behavior is likely associated with increased porosity and incomplete densification in these compositions, which is consistent with the microstructural features observed in the FE-SEM images (Figure 5). The presence of pores can enhance local electric field concentration, thereby promoting premature dielectric breakdown.

The close correlation between the structural and electrical properties provides further insight into the microscopic origin of the enhanced dielectric and ferroelectric responses in the CZ- and SZ-modified PFN–PT ceramics. According to the Rietveld refinement results, the maximum dielectric constant and remanent polarization obtained at x = 0.04 coincide with the reduced monoclinic lattice distortion, as evidenced by the smallest Δ (= |a − b|) and the β angle approaching 90°, indicating that this composition is located closest

[DOI: 10.22068/ijmse.4601]

to the morphotropic phase boundary (MPB). The incorporation of Ca^{2+} (or Sr^{2+}) together with Zr^{4+} subtly modifies the effective tolerance factor and relaxes the lattice distortion while maintaining the perovskite framework. This structural relaxation can lower the energy barrier associated with polarization rotation and facilitate ferroelectric domain switching, thereby enhancing the dielectric and ferroelectric properties. Although both modifiers induce a similar structural evolution, the consistently higher dielectric constant of the CZ-modified ceramics suggests that $CaZrO_3$ provides a slightly more favorable local structural environment for polarization development compared with $SrZrO_3$.

4. CONCLUSIONS

This study systematically investigated the structural, dielectric, and ferroelectric properties of (1–x)PFN–PT/x(Ca,Sr)ZrO_3 ceramic composites. X-ray diffraction and Rietveld refinement analyses revealed the structural evolution from a distorted monoclinic symmetry toward a pseudocubic structure with increasing CZ and SZ content, indicating the composition range near the morphotropic phase boundary (MPB). The optimized properties were achieved at x = 0.04, where the reduced lattice distortion was accompanied by enhanced dielectric permittivity and remanent polarization. The improved functional properties are attributed to the favorable structural state near the MPB, which promotes domain switching and enhances the ferroelectric response. Moreover, the different effects of CZ and SZ modification suggest that the type of A-site/B-site substitution plays an important role in tailoring the local structural environment and electrical performance of PFN–PT ceramics. These findings demonstrate that compositional engineering through $CaZrO_3$ and $SrZrO_3$ modification is an effective approach for optimizing the functional properties of PFN–PT-based multiferroic ceramics and provides useful guidelines for the development of advanced multifunctional electronic materials.

Statements & Declarations

Funding; The authors declare that no funds, grants, or other support were received during the preparation of this manuscript.

Conflicts of Interest; The authors have no relevant financial or non-financial interests to disclose.

Declaration of generative AI and AI-assisted technologies; The author declares that no generative AI or AI-assisted technologies were used in the writing process of this manuscript.

[DOI: 10.22068/ijmse.4601]

References

[1] Rödel, J., Kounga, A. B. N., Weissenberger-Eibl, M., Koch, D., Bierwisch, A., Rossner, W., Hoffmann, M. J., Danzer, R., & Schneider, G., "*Development of a roadmap for advanced ceramics: 2010–2025*", J. Eur. Ceram. Soc., 2009, 29, 1549–1560.

[2] Zeb, A., & Milne, S.J., "*High temperature dielectric ceramics: a review of temperature-stable high-permittivity perovskites*", J. Mater. Sci.: Mater. Electron., 2015, 26, 9243–9255.

[3] Yuan, X., Geng, X.Y., Zhang, J., Wang, R.X., Deng, X.Z., Sun, L., Gu, Z.B., & Zhang, S.T., "*$Bi_{0.5}Na_{0.5}TiO_3$-$BaTiO_3$-$CaZrO_3$: ZnO high-temperature dielectric composites with wide operational range*", Ceram. Int., 2018, 44, 12389–12394.

[4] Liu, Z., Fan, H., Lei, S., Ren, X., & Long, C., "*Duplex structure in $K_{0.5}Na_{0.5}NbO_3$-$SrZrO_3$ ceramics with temperature-stable dielectric properties*", J. Eur. Ceram. Soc., 2017, 37, 115–122.

[5] Wu, J., Xiao, D., & Zhu, J., "*Potassium–sodium niobate lead-free piezoelectric materials: past, present, and future of phase boundaries*", Chem. Rev., 2015, 115, 2559–2595.

[6] Ekhard, K.H., *Phase Transitions in Ferroelastic and Co-elastic Crystals: An Introduction for Mineralogists, Material Scientists and Physicists*. Cambridge University Press, 1990.

[7] Dang, P., He, C., Li, X., Han, S., Pan, S., & Long, X., "*A new multiferroic ternary solid solution system: $NdFeO_3$–$Pb(Fe_{1/2}Nb_{1/2})O_3$–$PbTiO_3$*", Ceram. Int., 2016, 42, 9347–9353.

[8] Wang, J., Tang, X. G., Chan, H. L. W., Choy, C. L., & Luo, H., "*Dielectric relaxation and electrical properties of $0.94Pb(Fe_{1/2}Nb_{1/2})O_3$–$0.06PbTiO_3$ single crystals*", Appl. Phys. Lett., 2005, 86, 152902.

[9] Singh, S. P., Singh, A. K., Pandey, D., Sharma, H., & Parkash, O., "*Crystallographic phases, phase transitions, and barrier layer formation in (1-x)[$Pb(Fe_{1/2}Nb_{1/2})O_3$]-x$PbTiO_3$*", J. Mater. Res., 2003, 18, 2677–2687.

[10] Suh, D.-H., Lee, D.-H., & Kim, N.-K., "*Phase developments and dielectric/ferroelectric responses in the PMN–PT system*," J. Eur. Ceram. Soc,, 2002, 22, 219–223.

[11] Dabkowski, A., Dabkowska, H. A., Greedan, J. E., Ren, W., & Mukherjee, B. K., "*Growth and properties of single crystals of relaxor PZN–PT materials obtained from high-temperature solution*", J. Cryst. Growth., 2004, 265, 204–213.

[12] Sitalo, E. I., Raevski, I. P., Lutokhin, A. G., Blazhevich, A. V., Kubrin, S. P., Raevskaya, S. I., Zakharov, Y. N., Malitskaya, M. A., Titov, V. V., & Zakharchenko, I. N., "*Dielectric and piezoelectric*

[DOI: 10.22068/ijmse.4601]

properties of $PbFe_{1/2}Nb_{1/2}O_3$-$PbTiO_3$ ceramics from the morphotropic phase boundary compositional range", IEEE Trans. Ultrason. Ferroelectr. Freq. Control., 2011, 58, 1914–1919.

[13] Ramani, G. V. & Agrawal, D. C., "*Stabilization of the perovskite phase and dielectric properties in $Pb(Zn_{1/3}Nb_{2/3})O_3$-$Pb(Fe_{1/2}Nb_{1/2})O_3$ relaxor ferroelectrics*", Ferroelectrics., 1993, 150, 291–301.

[14] Yokosuka, M., "*Electrical, electromechanical and structural studies on solid solution ceramic $Pb(Fe_{1/2}Nb_{1/2})O_3$–$Pb(Zn_{1/3}Nb_{2/3})O_3$*", Jpn. J. Appl. Phys., 1999, 38, 5488.

[15] Sunder, V. V. S. S. S. & Umarji, A. M., "*Thermal expansion studies in the lead iron niobiate—Lead titanate system*", Mater. Res. Bull., 1995, 30, 427–434.

[16] Singh, S. P., Yusuf, S. M., Yoon, S., Baik, S., Shin, N., & Pandey, D., "*Ferroic transitions in the multiferroic $(1-x)Pb(Fe_{1/2}Nb_{1/2})O_3$–$xPbTiO_3$ system and its phase diagram*", Acta Mater., 2010, 58, 5381–5392.

[17] Zhou, Z., Tang, H., & Sodano, H. A., "*Scalable synthesis of morphotropic phase boundary lead zirconium titanate nanowires for energy harvesting*", Adv. Mater., 2014, 26, 7547–7554.

[18] Zhao, W., Zuo, R., Li, F., & Li, L., "*Structural, dielectric, ferroelectric and strain properties in $CaZrO_3$-modified $Bi(Mg_{0.5}Ti_{0.5})O_3$–$PbTiO_3$ solid solutions*", J. Alloys Compd., 2014, 591, 218–223.

[19] Goldschmidt, V. M., "*Die gesetze der krystallochemie, Naturwissenschaften*", 1926, 14, 477–485.

[20] Guo, H., Shimizu, H., Mizuno, Y., & Randall, C. A., "*Strategy for stabilization of the antiferroelectric phase (Pbma) over the metastable ferroelectric phase (P21ma) to establish double 13loop hysteresis in lead-free $(1-x)NaNbO_3$-$xSrZrO_3$ solid solution*", J. Appl. Phys, 2015, 117, 214102.

[21] Yao, F.-Z., Glaum, J., Wang, K., Jo, W., R¨odel, J., & Li, J.-F., "*Fatigue-free unipolar strain behavior in $CaZrO_3$ and MnO_2 co-modified (K, Na)NbO_3-based lead-free piezoceramics*", Appl. Phys. Lett., 2013, 103, 192903.

[22] Shimizu, H., Guo, H., Reyes-Lillo, S. E., Mizuno, Y., Rabe, K. M., & Randall, C. A., "*Lead free antiferroelectric: $xCaZrO_3$-$(1-x)NaNbO_3$ system ($0 \leq x \leq 0.10$)*", Dalton Trans., 2015, 44, 10763–10772.

[23] Gong, S., Shi, K., Zhao, T.-L., Zhuang, J., Quan, Y., Sun, X., Jin, Y., Zhang, Y., Dong, G., Zhao, J., et al., "*High temperature piezoelectric performance of $CaZrO_3$ modified $BiScO_3$-$PbTiO_3$ ceramics*", Ceram. Int., 2024, 50, 43665–43673.

[DOI: 10.22068/ijmse.4601]

[24] Deng, X.-Z., Zhang, L.-Y., Geng, X.-Y., Zhang, J., Sun, L., Wang, R.-X., Gu, Z.-B., & Zhang, S.-T., "*Crystal structure, impedance, and multiferroic property of $SrZrO_3$ and MnO_2 modified 0.725$BiFeO_3$-0.275$BaTiO_3$ ceramics*", Ceram. Int., 2017, 43, 14748–14755.

[25] Huang, T., Xiao, D., Liu, C., Li, F., Wu, B., Wu, J., & Zhu, J., "*Effect of $SrZrO_3$ on phase structure and electrical properties of 0.974(K0.5Na0.5)NbO_3–0.026$Bi_{0.5}K_{0.5}TiO_3$ lead-free ceramics*", Ceram. Int., 2014, 40, 2731–2735.

[26] Tang, B., Zhang, S., Yuan, Y., Zhou, X., & Liang, Y., "*Influence of $CaZrO_3$ on dielectric properties and microstructures of $BaTiO_3$-based X8R ceramics*", Sci. China Ser. E: Technol. Sci., 2008, 51, 1451–1456.

[27] Yan, W., Xia, Z., Li, Q., & Zhang, S., "*Growth and electrical performance of $Pb(Mg_{1/3}Nb_{2/3})O_3$–$PbTiO_3$–$Pb(Fe_{1/2}Nb_{1/2})O_3$ single crystals*", Mater. Res. Bull., 2009, 44, 1256–1260.

[28] Xia, Z. & Li, Q., "*Structural phase transformation and electrical properties of (0.90-x)$Pb(Mg_{1/3}Nb_{2/3})O_3$–x$PbTiO_3$–0.10$Pb(Fe_{1/2}Nb_{1/2})O_3$ ferroelectric ceramics near the morphotropic phase boundary*", Acta Mater., 2007, 55, 6176–6181.

[29] Luo, N., Li, Q., Yan, Q., Zhang, Y., Xia, Z., & Chu, X., "*Structure, frequency dependent dielectric properties and domain configuration of PMN–PFN–PT single crystal*", J. Cryst. Growth., 2014, 401, 414–417.

[30] Xiao, J., Xu, L., Paix˜ao, J. A., & Costa, M. M. R., "*XAFS and Dielectric Study for $Pb(Fe_{1/2}Nb_{1/2})O_3$-$PbTiO_3$ Crystals*", Ferroelectrics, 2013, 448, 17–22.

[31] Pang, D., He, C., Han, S., Pan, S., Long, X., & Tailor, H., "*A new multiferroic ternary solid solution system of $BiFeO_3$–$Pb(Fe_{1/2}Nb_{1/2})O_3$–$PbTiO_3$*", J. Eur. Ceram. Soc., 2015, 5, 2033–2040.

[32] Luo, N., Li, Q., Xia, Z., & Chu, X., "*Phase Diagram, Temperature Stability, and Electrical Properties of (0.85-x)$Pb(Mg_{1/3}Nb_{2/3})O_3$–0.10$Pb(Fe_{1/2}Nb_{1/2})O_3$–0.05$PbZrO_3$–x$PbTiO_3$ System*", J. Am. Ceram. Soc., 2012, 95, 3246–3253.

[33] Fesharaki, M. J., Jalali, M. R., Karimi, L., & Sadeghi, E., "*UV excited thermoluminescence and kinetic analysis of $CaZrO_3$:xCe^{3+} phosphors synthesized by sol–gel combustion method*", Opt. Quantum Electron., 2023, 55, 1257.

[34] Zheng, T., Jiang, Z., & Wu, J., "*Enhanced piezoelectricity in (1-x)$Bi_{1.05}Fe_{1-y}AyO_3$–x$BaTiO_3$ lead-free ceramics: site engineering and wide phase boundary region*", Dalton Trans., 2016, 45, 11277–11285.

[DOI: 10.22068/ijmse.4601]

[35] Guo, Y., Xiao, P., Wen, R., Wan, Y., Zheng, Q., Shi, D., Lam, K. H., Liu, M., & Lin, D., "*Critical roles of Mn-ions in enhancing the insulation, piezoelectricity and multiferroicity of $BiFeO_3$-based lead-free high temperature ceramics*", J. Mater. Chem. C., 2015, 3, 5811–5824.

[36] L. Lutterotti, L., *"Maud: A Rietveld analysis program designed for the internet and experiment integration*," Acta Crystallogr. Sect. A: Found. Crystallogr. 2000, 56, S54.

[37] Shrout T.R., & Zhang, S.J., "Lead-free Piezoelectric Ceramics: Alternatives for PZT?, in Progress in Advanced Dielectrics", 2020, 295–327. World Scientific.

[38] Xi, Z., Bu, Q., Fang, P., Long, W., & Li, X., "*Effect of frequency and temperature on dielectric relaxation of [1 1 1]-oriented PMN-32PT single crystals*", J. Alloys Compd., 2015, 618, 14–18.

[39] Jan, S. Q., Usman, M., Naveed-Ul-Haq, M., & Mumtaz, A., "*A study of relaxation effects in (1-x)$BaZr_{0.2}Ti_{0.8}O_3$-x$Ba_{0.7}Ca_{0.3}TiO_3$ (x=0.3, 0.35, 0.4) ferroelectric ceramics*", J. Alloys Compd, 2018, 735, 1893–1900.

[40] Usman, M., Mumtaz, A., Raoof, S., & Hasanain, S. K., "*Magnetic control of relaxor features in $BaZr_{0.5}Ti_{0.5}O_3$ and $CoFe_2O_4$ composite*", Appl. Phys. Lett., 2013, 102, 112905.

[41] Bilić, A. & Gale, J. D., "*Proton mobility in the In-Doped $CaZrO_3$ perovskite oxide", Chem. Mater*., 2007, 19, 2842–2851.

[42] Weston, L., Janotti, A., Cui, X. Y., Stampfl, C., & Van de Walle, C. G., "*Acceptor doping in the proton conductor $SrZrO_3$*", Phys. Chem. Chem. Phys., 2017, 19, 11485–11491.

[43] Gu, J., Sun, X., Jiang, L., Zhang, Z., Norby, T., & Han, D., "*Surface protonic conduction in porous alkaline earth zirconate perovskites $CaZrO_3$, $SrZrO_3$, and $BaZrO_3$*", J. Mater. Chem. A., 2024, 12, 26555–26567.

[44] Wang, B., Li, Y., & Hall, D. A., "*Surface structure and quenching effects in $BiFeO_3$-$BaTiO_3$ ceramics*", J. Am. Ceram. Soc., 2022, 105, 1265–1275.

[DOI: 10.22068/ijmse.4601]